THE EFFECT OF PARTICLE INTRUSION ON RAIL SEAT LOAD DISTRIBUTIONS ON HEAVY HAUL FREIGHT RAILROADS

Matthew J. Greve
Graduate Research Assistant
University of Illinois at Urbana-Champaign, Illinois, USA

Marcus S. Dersch
Senior Research Engineer
University of Illinois at Urbana-Champaign, Illinois, USA

J. Riley Edwards
Research Scientist and Senior Lecturer
University of Illinois at Urbana-Champaign, Illinois, USA

Christopher P.L. Barkan
Professor and Executive Director of RailTEC
University of Illinois at Urbana-Champaign, Illinois, USA

Jose Mediavilla
Director of Engineering – Fasteners
Amsted RPS, Kansas, USA

Brent Wilson
Director of Research and Development
Amsted Rail, Illinois, USA

SUMMARY

The rail seat load distribution is critical to the analysis of failure mechanisms associated with rail seat deterioration (RSD), the degradation of the concrete surface at the sleeper rail seat. RSD can lead to wide gauge, cant deficiency, and an increased risk of rail rollover, and is therefore of primary concern to heavy haul freight railroads in North America. Previous experimentation with MBTSS at the University of Illinois at Urbana-Champaign (UIUC) has yielded concern regarding the feasibility of crushing of the concrete material at the rail seat as a failure mechanism associated with RSD. This paper examines data collected from laboratory experimentation in which the particle size, extent of particle intrusion, vertical rail seat load, and lateral over vertical force ratio were varied to generate realistically extreme loading environments. Matrix based tactile surface sensors (MBTSS) were used to collect the distribution of loads at the sleeper rail seat. No pressures were recorded that exceeded the minimum theoretical threshold to initiate crushing, but extreme loading scenarios yielded pressures exceeding the fatigue strength of the concrete rail set. It was therefore concluded that although crushing damage due to a single load application is not expected, accumulated crushing damage due to a high number of repeated load applications may be a feasible failure mechanism by which RSD may be initiated.

1. INTRODUCTION

As the demand in North America for high-performance, low-maintenance railroad infrastructure continues to grow, concrete sleepers and elastic fastening systems are becoming increasingly common. Concrete sleepers are typically used in areas of high curvature and steep grades on lines that experience high-speed or heavy-axle load traffic [1]. Because of the increasingly common application of concrete sleepers and elastic fastening systems in these high-demand environments, it is important to understand the factors contributing to common performance failures of concrete sleepers and fastening systems. One of the most common failures of concrete sleepers is the degradation of the concrete material directly below the rail, in the area of the sleeper known as the rail seat. This degradation is commonly referred to as rail seat deterioration (RSD), or rail seat abrasion (RSA) [2]. Figure 1 illustrates a typical instance of RSD, with the depth of wear increasing towards the field side of the rail seat. RSD has become a problematic failure for concrete sleepers since it was first observed in the 1980's, and is often found in regions of steep grades, high curvature, and in the presence of moisture [1]. If left untreated, RSD may lead to accelerated wear of the fastening system, wide gauge, excessive rail cant, and an increased risk of derailment due to rail rollover [1].

Figure 1: Typical Rail Seat Deterioration (RSD) Wear Pattern

According to a survey of North American railroad industry representatives, RSD is considered the most critical problem with concrete sleepers and fastening systems. Additionally, it was ranked as the area of sleeper and fastening system research most in need of research [3]. As part of a larger research project funded by the Federal Railroad Administration (FRA) investigating common failures with concrete sleepers and elastic fastening systems, researchers at the University of Illinois at Urbana-Champaign (UIUC) are investigating the failure modes associated with RSD. Previous research has identified five failure mechanisms that may result in RSD: abrasion, crushing, freeze-thaw cracking, hydro-abrasive erosion, and hydraulic pressure cracking [1]. Of these five failure mechanisms, four are affected by the distribution of loads on the sleeper rail seat, the exception being freeze-thaw cracking. Therefore, researchers at UIUC have undertaken an effort to better understand the distribution of the rail seat load, the factors that affect it, and its effect on rail seat deterioration. Previous research has highlighted the effect of pad modulus, fastening system type, loading environment, RSD, and fastener wear on the rail seat load distribution [4,5,6,7]. Researchers at UIUC hope to incorporate the findings on RSD failure mechanisms with findings from other research to generate a framework for the mechanistic design of concrete sleepers and their fastening systems, in which components are designed from expected outputs and observed relationships. It is believed that such a design approach would establish a clearer procedure for designing sleepers and fastening systems, resulting in fewer service failures and higher reliability of the track structure and its components [8].

2. NOTATION

FRA	Federal Railroad Administration
L/V	Lateral/Vertical Force Ratio
MBTSS	Matrix-Based Tactile Surface Sensors
PLTM	Pulsating Load Testing Machine
RAIL	Research and Innovation Laboratory
RSA	Rail Seat Abrasion
RSD	Rail Seat Deterioration
Volpe	Volpe National Transportation Systems Center
UIUC	University of Illinois at Urbana-Champaign
UK	University of Kentucky

3. CRUSHING AS AN RSD FAILURE MECHANISM

Crushing is defined as damage to the sleeper rail seat resulting from pressures exceeding the strength of the concrete material [1]. In North America, the minimum recommended design 28-day compressive strength is 48 MPa (7,000 psi) [2]. However, practical experience has shown that the achieved 28-day compressive strength can exceed 76 MPa (11,000 psi) [1].

Experimentation conducted at the Volpe National Transportation Systems Center (Volpe) suggests that crushing may be a feasible failure mechanism for RSD. To investigate several passenger train derailments caused by RSD, Volpe utilized a NUCARS™ model to obtain the magnitudes of vertical and lateral load and location of the wheel/rail contact patch. This information was then applied to an empirical model which treats the rail as a footing on an elastic foundation. The findings of this research suggest that pressures exceeding 110 MPa (16,000 psi) may be possible [9]. However, the analysis was performed under several “worst-case” assumptions. The analysis neglected the rotational restraint provided by the elastic fasteners, and assumed that the rail pad provided no distribution of load from the rail. These assumptions may therefore not accurately represent typical field conditions, and may simulate only the most extreme cases of RSD and fastening system deterioration. Further, previous research conducted at UIUC has not revealed evidence of rail seat pressures exceeding 30 MPa (4,400 psi), far below the minimum theoretical threshold for crushing, 48 MPa (7,000 psi) [4,5,6,7]. Experimentation was therefore undertaken with matrix-based tactile surface sensors (MBTSS) to generate extreme rail seat pressures via particle intrusion at the sleeper rail seat.

4. INSTRUMENTATION TECHNOLOGY

To characterize the distribution of load at the sleeper rail seat, researchers at UIUC have utilized MBTSS. The MBTSS system used by UIUC is manufactured by Tekscan® Inc. and consists of rows and columns of conductive ink which, when pressed together by a load applied normal to the contact plane, output a change in resistivity at each intersection of a row and a column. This output, termed a “raw sum”, can be interpreted as the pressure exerted on the sensor at a given intersection when given the total applied load. MBTSS simultaneously outputs the area over

which this load is applied. This is termed the "contact area" of the load and is calculated from the number of sensing locations that indicate an applied load. Data are collected from the entire sensing area at a maximum rate of 100 Hz. The data are calibrated during analysis using a known or assumed input load.

Previous experimentation at the University of Kentucky (UK) and UIUC has shown that MBTSS are susceptible to shear and puncture damage. To protect the sensors, layers of biaxially-oriented polyethylene terephthalate (BoPET) and polytetrafluoroethylene (PTFE) are secured to both sides of a sensor that has been trimmed to fit the rail seat. The assembly is then installed between the rail pad assembly and the concrete sleeper rail seat (Figure 2) [10].

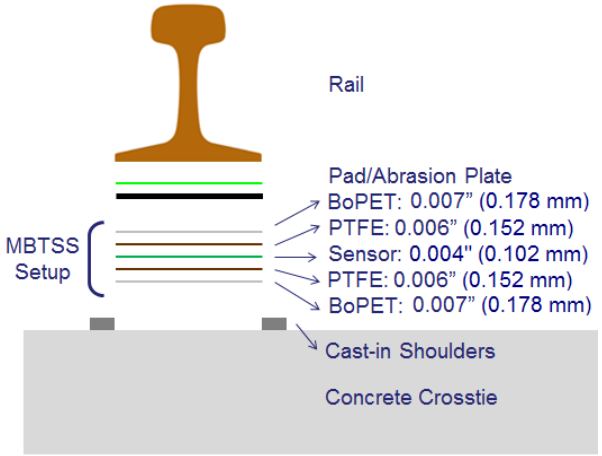

Figure 2: MBTSS Layers and Thicknesses [10]

5. LABORATORY EXPERIMENTATION

Experimentation was conducted at UIUC's Research and Innovation Laboratory (RAIL) at Schnabel utilizing the Pulsating Load Testing Machine (PLTM), which is owned by Amsted RPS. The PLTM is a bi-axial loading frame designed to perform AREMA Test 6, a Wear and Abrasion test, on a single rail seat with a complete fastening system assembly. The PLTM is equipped with one vertically-oriented 245 kN (55,0000 lb) actuator and one laterally-oriented 156 kN (35,000 lb) actuator. The actuators can be controlled independently by either force or displacement. For these experiments, force control was used.

In order to develop an experimental matrix which would generate extreme rail seat pressures, the size and amount of particles applied to each rail seat were varied. Locomotive sand was used to represent typical particle intrusion, as practical experience and the AREMA Test 6 procedure indicate that particles typically found at the rail pad-rail seat interface are of comparable size. To generate more extreme pressures, virgin Class B crushed stone ("B-Stone") aggregate from the UIUC concrete laboratory was used to simulate debris from deterioration of the concrete at the rail seat. Figure 3 shows the grain size distribution of the aggregate after all material retained at or above the #4 sieve was removed (14% of the total sample by weight).

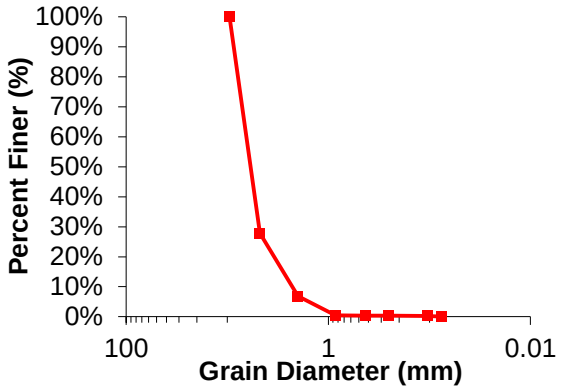

Figure 3: Concrete Aggregate Grain Size Distribution

Previous experimentation has shown that the portion of the rail seat not more than 2.54 cm (1 in) from the field side shoulder is the region of the rail seat which is most sensitive to changes in the rail seat load distribution [7]. Therefore, it was decided to also vary the portion of the rail seat over which the particles were applied. To represent typical particle intrusion, 15 mL (3 teaspoons) of material were distributed evenly over the entire rail seat.

To simulate a more extreme case, 2.5 mL (0.5 teaspoons) of material were distributed evenly over the 2.54 cm (1 in) of the rail seat closest to the field side, as described above. It was hypothesized that this uneven distribution of particles would create an effective difference in height across the rail seat, resulting in a greater proportion of the rail seat load imparted on the area of the rail seat already known to be most sensitive to changes in rail seat load. This combination of particle size and region of intrusion leads to five experimental cases: No Fines (the control case), 1" Sand (sand applied to the field-side inch of the rail seat), Full Sand (sand applied to the entire rail seat), 1" Aggregate (B-Stone aggregate applied to the field-side inch of the rail seat), and Full Aggregate (B-Stone aggregate applied to the entire rail seat).

In field conditions, it is rare that a single rail seat will carry the entire vertical load applied by a single wheel. Instead, the vertical wheel load is often distributed across five or more sleepers, with the rail seat directly below the point of loading carrying the largest proportion of the load [11]. An extensive literature review and previous field experimentation have shown that average values for the rail seat load directly below point of loading are typically close to 50% of the total vertical wheel load. However, this value may vary significantly, predominately due to the support conditions under the rail seat in relation to that of neighboring rail

seats [8]. The magnitude of vertical load applied in this experimentation was therefore varied to capture this behavior, with testing conducted at 44.5 kN (10,000 lb), 88.9 kN (20,000 lb), and 133 kN (30,000 lb). These values were chosen to represent 25%, 50%, and 75% of 178 kN (40,000 lb), which represents a 95th percentile nominal vertical wheel load in North American heavy haul freight service [3]. At each magnitude of vertical load, the Lateral/Vertical (L/V) Force Ratio was also varied from 0.0 to 0.6, to simulate varying degrees of curvature.

The Amsted RPS P2000 fastening system was used in this experimentation. All clips were applied new, and discarded when removed to eliminate variability due to reduced toe load from fastener wear. The same two-part pad assembly and insulators were used for all experimentation to eliminate thickness variations within manufacturing tolerances. The pad assembly and insulators were lightly used in previous experimentation but were undamaged prior to installation. Before each application of particles, the rail seat was cleaned with a handheld broom to prevent contamination from the prior particle intrusion case (e.g. removing sand prior to experimentation with aggregate). Three separate trials were conducted for each combination of particle size, intrusion region, vertical load, and lateral load. The results presented in this paper represent an average of the three corresponding data points, except as noted. Replicates were collected to assess the variability induced by particle intrusion, but the rail seat load distribution was found to behave consistently for repeated trials with identical experimental conditions.

6. RESULTS

During experimentation, researchers noted that the presence of aggregate at the rail seat significantly increased the difficulty of assembling the fastening system. Due to the effective increase in height of the rail base above the rail seat, the insulators developed a tendency to become unseated during clip application. Additional rotational restraint of the rail was required to enable the application of both fasteners. Upon disassembly of the fastening system following experimentation with the crushed stone aggregate, the particles were found to have been pulverized during experimentation, resulting in reduced particle size as shown in Figure 4. Despite the pulverization of the aggregate, the qualitative behavior of the rail seat load distribution did not appear to change as a result of the effective decrease in particle size. Due to the small sample size, a sieve analysis was not run on the pulverized material.

In order to prevent failure of the fastening system, experimentation was halted when the rail seat load became concentrated solely on the half of the rail seat closest to the field side shoulder (i.e. if the gauge side of the rail seat was completely unloaded). Experience has shown high lateral loads tend to result in this concentration, which precedes the plastic yield-failure of the gauge side clip. This threshold was reached at approximately 0.56 L/V force ratio under a 133 kN (30,000 lb) vertical load during experimentation both with no fines present and in the Full Sand case. When aggregate was placed on the field side of the rail seat, the target 0.6 L/V force ratio was achieved at all three tested vertical load magnitudes. It is hypothesized that the improved tolerance of high lateral loads was due to an effective increase in rail cant caused by the aggregate elevating the field side of the rail base. When aggregate was placed on the entire rail seat, experimentation was halted at 0.58 L/V under an 88.9 kN (20,000 lb) vertical load and 0.5 L/V under a 133 kN (30,000 lb) vertical load due to the previously described unloading of the gauge side. It is hypothesized that the effective increase in height of the rail base, which led to the aforementioned difficulty with assembling the fastening system, may have changed the magnitude and direction of the resultant force applied by the fastener toe load, leading to a decrease in rail rotational restraint.

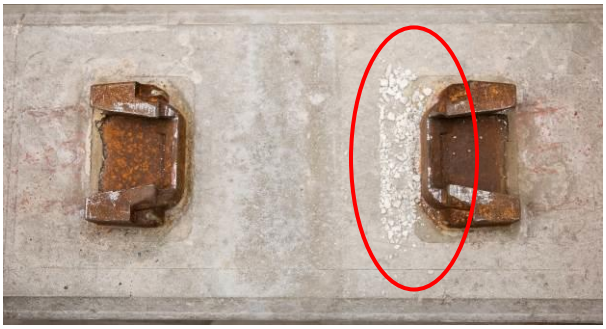

(a)

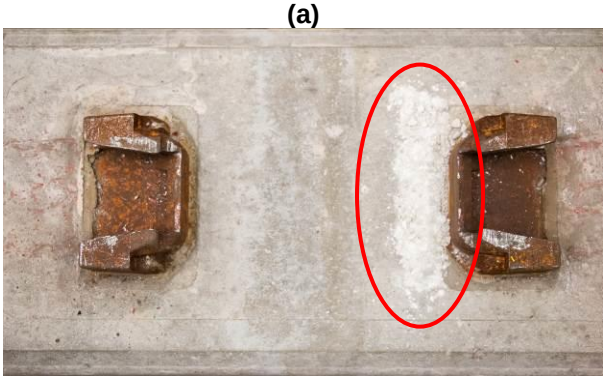

(b)

Figure 4: Aggregate (Circled) Before (a) and After (b) 1" Aggregate Experiments

6.1. Qualitative Analysis

Figure 5 compares the qualitative effect of both L/V force ratio and particle intrusion on rail seat load distributions. The first series represents the common design assumption that the rail seat load is distributed uniformly across the entirety of a clean sleeper rail seat. By definition, this

assumption does not account for changes in L/V force ratio. The remaining five series illustrate each of the experimental cases for particle intrusion: clean rail seat (no particle intrusion), sand intrusion on the field side of the rail set, sand intrusion on the entire rail seat, aggregate intrusion on the field side of the rail seat, and aggregate intrusion on the entire rail seat.

A nonuniform distribution of load was observed in all five experimental cases, with the variation in particle size and extent of intrusion affecting the magnitude of nonuniformity. The primary effect of particle size was on regularity of the load distribution. Larger aggregate particles produced greater variation in measured load at adjacent sensing locations, as represented by the "peaks" of warmer colors evident in the Full Aggregate case. The primary effect of the extent of particle intrusion was on the portion of load applied to the region of the rail seat not more than 2.54 cm (1 in) from the field side shoulder. The intrusion of particles exclusively in this region leads to a gap in the load distribution at lower L/V's that is not present under the intrusion of particles across the entire rail seat. Moreover, experimentation with sand particles suggests that in the 1" Sand case, a greater portion of the rail seat load was applied to the field side of the rail seat than in the Full Sand case.

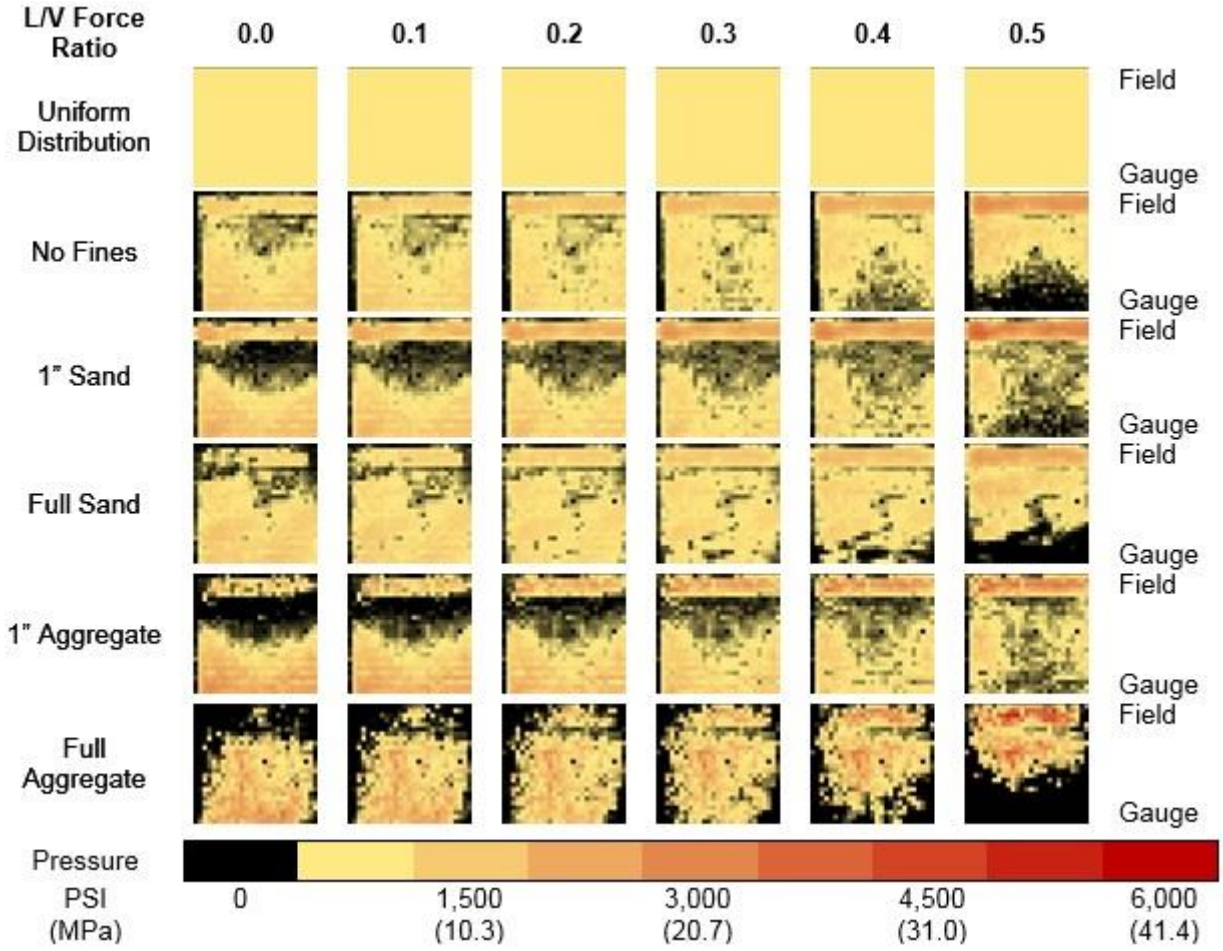

Figure 5: Qualitative Comparison of Rail Seat Load Distributions under 133 kN (30 kip) Vertical Wheel Load at Varying L/V Force Ratios

6.2. Quantitative Analysis

Figure 6 summarizes the effect of particle intrusion on contact area (the area over which the rail seat load is distributed) when subjected to increasing L/V force ratio under a constant 133 kN (30,000 lb) vertical load. In the No Fines, 1" Sand, and Full Sand cases, more than 90% of the rail seat is engaged at low L/V force ratios. The contact area remains relatively constant until 0.4 L/V force ratio is reached, with the presence of sand introducing slightly higher contact areas than the No Fines case. Beyond 0.4 L/V force ratio, the three cases experienced a rapid loss of contact area. When experimentation was halted at approximately 0.56 L/V force ratio, the No Fines, 1" Sand, and Full Sand cases exhibited a 38%, 33%, and 43% reduction in contact area, respectively, relative to the contact area observed at 0.0 L/V force ratio for each case.

As shown qualitatively in Figure 5, the presence of aggregate at the concrete sleeper rail seat generates an overall reduction in contact area. Both aggregate cases exhibited a lower initial contact area at 0.0 L/V force ratio. Only 80% of the total rail seat area was loaded in the 1" Aggregate case, and only 69% was loaded in the Full Aggregate case. Both aggregate cases then showed a gradual increase in contact area before reaching a critical L/V force ratio. Beyond this threshold, both experimental cases exhibited rapid reductions in contact area. In the 1" Aggregate case, contact areas comparable to those observed in the No Fines case were achieved between 0.3 and 0.5 L/V force ratio. As previously mentioned, the 1" Aggregate case was the only experimental case to achieve the target L/V force ratio of 0.6 L/V under a 133 kN (30,000 lb) vertical load, at which point the contact area was measured to be 37% less than that at 0.5 L/V force ratio. The Full Aggregate case, by comparison, achieved a maximum contact area 21% lower than the contact area observed on a clean rail seat. When experimentation was halted at 0.5 L/V force ratio, the Full Aggregate case exhibited 44% less contact area than that observed at 0.0 L/V force ratio in the No Fines case.

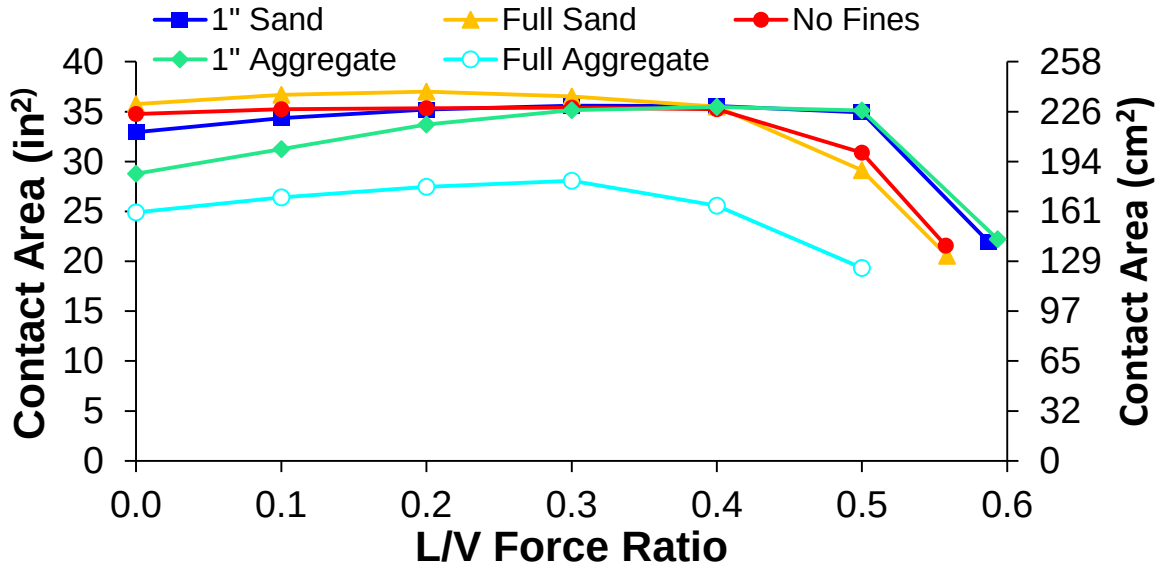

Figure 6: Loss of Contact Area under 133 kN (30,000 lb) Vertical Load

Figures 7 and 8 quantify the change in pressure as a result of the experimentation. There are three primary metrics by which rail seat pressures are typically analyzed: theoretical uniform pressure, average pressure, and maximum pressure. The theoretical uniform pressure is obtained by dividing the total rail seat load by the total rail seat area, and represents the common design assumption that the rail seat load is uniformly distributed across the entirety of the sleeper rail seat. The theoretical uniform pressure is included in both Figures 7 and 8, and serves as a comparison between the data and the theoretical, uniform case. The average pressure is obtained by dividing the total rail seat load by the measured contact area, rather than the total rail seat area as used to calculate the theoretical uniform pressure. The maximum pressure is the highest pressure recorded by the MBTSS at any combination of vertical load and L/V force ratio.

Figure 7 illustrates the effect of particle intrusion and L/V force ratio on the average rail seat pressure. Because average pressure is derived from contact area, the data series exhibit inverse behavior when compared to the contact area data illustrated in Figure 6 (i.e. higher contact areas correlate to lower average pressures). Because the No Fines, 1" Sand, and Full Sand cases result in almost all of the rail seat being engaged in load transfer at low L/V force ratios, the average pressures plot very close to the theoretical uniform pressure. Below the aforementioned threshold of 0.4 L/V force ratio, the three cases yielded average pressures within 10% of the theoretical uniform pressure. As contact area decreased above this threshold, the No Fines, 1" Sand, and Full Sand cases experienced an increase in average pressure of 61%, 51%, and 75%, respectively, resulting in average pressures 67%, 65%, and 77% higher than the theoretical uniform pressure, respectively.

Due to the reduced contact area measured in the presence of aggregate at the sleeper rail seat, the 1" Aggregate and Full Aggregate cases exhibited slightly higher pressures than those observed on a clean rail seat or in the presence of sand. As contact area increases from 0.0 to 0.3 L/V force ratio for the 1" Aggregate case, the average pressure was reduced from 25% higher than the theoretical uniform pressure to just 3% higher.

Following the loss of contact area from 0.5 to 0.6 L/V force ratio, the average pressure increased 59%, resulting in an average pressure 30% higher than the theoretical uniform pressure. In the Full Aggregate case, the average pressure at 0.0 L/V force ratio was 45% higher than the theoretical uniform pressure before experiencing a reduction as increasing L/V force ratio resulted in a greater portion of the rail seat engaged in load transfer. At 0.3 L/V, the average pressure observed in the Full Aggregate case was 30% higher than the theoretical uniform pressure, before again increasing as contact area was lost. At 0.5 L/V force ratio, when experimentation was halted, the Full Aggregate case had experienced an overall increase in pressure of 31%, resulting in values 90% higher than the theoretical uniform pressure.

Figure 8 illustrates the effect of particle intrusion and L/V force ratio on the maximum rail seat pressure. While the presence of sand resulted in contact areas slightly higher than those observed in the No Fines case, Figure 5 shows significant areas of the rail seat engaged in load transfer at lower pressures in the 1" Sand case. This therefore leads to higher maximum pressures than those seen in the No Fines and Full Sand cases. While maximum pressures in the Full Sand case are comparable to those observed in the No Fines Case, increasing from 2.6 to 5 times the theoretical uniform pressure between 0.0 and 0.56 L/V force ratio, maximum pressures recorded in the 1" Sand case ranged from 3.1 to 7.1 times the theoretical uniform pressure at 0.0 and 0.58 L/V force ratio, respectively. The 1" Aggregate case resulted in behavior similar to the 1" Sand case, with maximum pressures ranging from 3.7 to 7.3 times the theoretical uniform pressure at 0.0 and 0.6 L/V, respectively. The Full Aggregate case consistently exhibited the highest maximum pressures at any given L/V force ratio, ranging from 4.8 to 7.7 times the theoretical uniform pressure at 0.0 and 0.5 L/V, respectively.

The highest pressure recorded during experimentation were observed in the Full Aggregate case, with a maximum pressure of approximately 44 MPa (6,400 psi), achieved at 0.5 L/V force ratio, respectively. It is hypothesized that crushing of the B-Stone aggregate occurred at these high L/V force ratios, leading to reduced particle size which, in turn, led to similar results to the 1" Sand case at high L/V force ratios. Had the aggregate particles not failed, it is feasible that higher maximum pressures could have been observed. Further experimentation with stronger aggregate is needed to evaluate this hypothesis. The sensing resolution of the MBTSS also presents a limitation. Each sensing location is 0.56 cm (0.22 in) square. It is possible that there may be regions smaller than the size of a single sensing location where the applied pressure may be higher than those observed in this study. Due to the limitations of the instrumentation, however, the data reflect the average pressure applied to each 0.31 cm^2 (0.0484 in^2) sensing location. Nonetheless, because the observed maximum pressures fall short of the design compressive strength of concrete used in the manufacture of concrete sleepers in North America (48 MPa), crushing damage due to a single load application is not expected in the presence of particle intrusion on a concrete rail seat with a new fastening system.

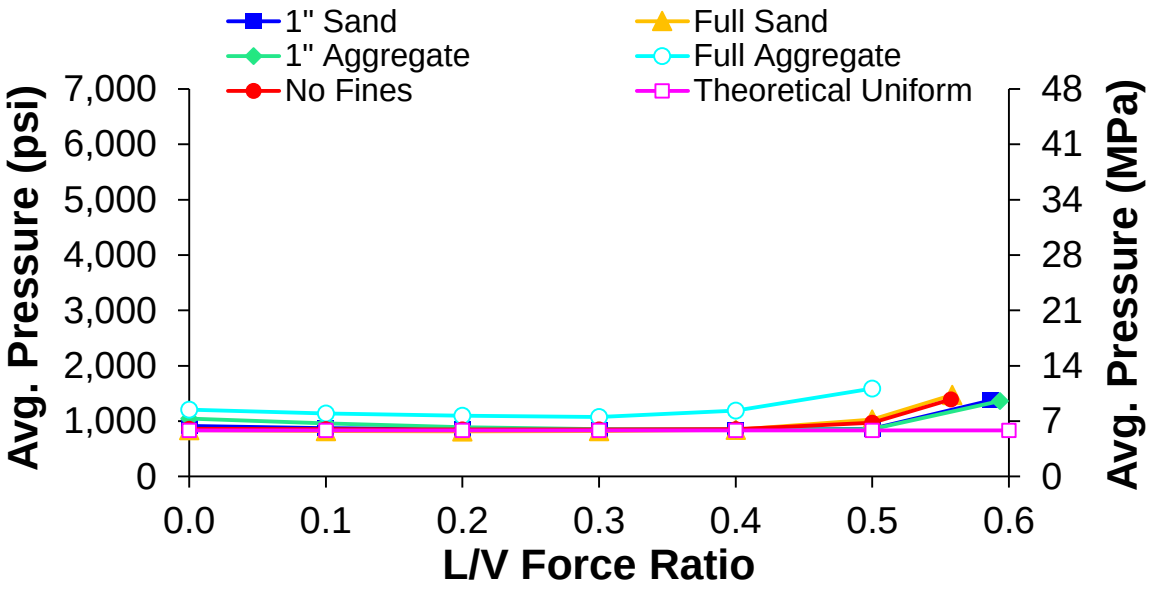

Figure 7: Increase in Average Pressure under 133 kN (30 kip) Vertical Load

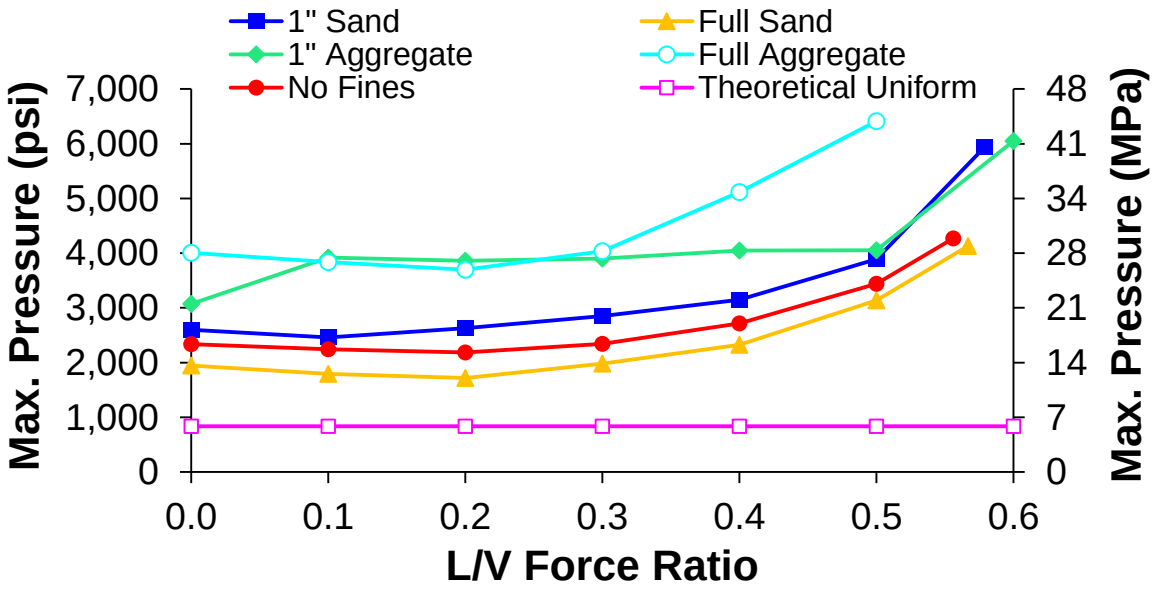

Figure 8: Increase in Maximum Pressure under 133 kN (30 kip) Vertical Load

While this experimentation did not generate pressures exceeding the design compressive strength of the concrete, crushing damage as a result of repeated load applications may be feasible. The fatigue compressive strength of concrete is generally regarded as ranging from 50 to 60% of the ultimate compressive strength for high-load cycle applications [12, 13]. A conservative estimate of the design fatigue compressive strength of concrete would therefore be 24 MPa (3,500 psi), or half of the design compressive strength. Figure 8 shows that at high L/V force ratios (above 0.4), the maximum pressures observed in the 1" Sand, 1" Aggregate, and Full Aggregate cases exceeded this threshold. This indicates that crushing damage to the concrete rail seat as a result of repeated load applications may indeed be feasible in cases of extreme particle intrusion and high rail seat loads.

Practical experience has shown that the actual compressive strength achieved in the manufacture of North American concrete sleepers can exceed 76 MPa (11,000 psi), nearly twice the highest pressure observed in this experimentation. Further, the reported concrete compressive strength is obtained from compressive tests on unreinforced concrete cylinders [2]. The confinement provided by the mass of concrete comprising the rail seat and the prestress provided by the sleeper reinforcement will further increase the actual compressive strength of the concrete at the sleeper rail seat, further increasing the pressure necessary to generate crushing. Although these factors further indicate that crushing due to a single load application may not be feasible, the data shown in Figure 8 suggest that crushing due to repeated load application may still be feasible in the most extreme cases (e.g. particle intrusion only on the field side of the rail seat). Further, previous laboratory experimentation has shown that fastener wear can lead to an increase in rail seat pressures [7]. In such cases, the accumulation of crushing damage to the concrete rail seat may be accelerated by the increase in maximum pressures.

7. CONCLUSION

In this experimentation, particle size, extent of intrusion, vertical rail seat load, and L/V force ratio were varied to generate realistically demanding loading environments. The distribution of loads at the sleeper rail seat was collected using matrix-based tactile surface sensors, and the data were analyzed to determine the effect of particle intrusion. While the presence of sand had little effect on the measured contact area, the presence of aggregate led to an average reduction of 23% at 0.0 L/V force ratio. An average 35% reduction in contact area due to high L/V force ratios was observed in all experimental cases. No average pressures were observed to be greater than 200% of the theoretical average pressure given a uniform distribution of rail seat load. While maximum pressures of 44 MPa (6,400 psi) were recorded, the minimum threshold to generate crushing, a proposed failure mechanism for RSD, as a result of a single load application, was not exceeded. In extreme loading cases, however, the estimated design fatigue strength of the concrete, 24 MPA (3,500 psi) was exceeded. These findings indicate that crushing damage may be generated as a result of a large number of repeated load applications. It was therefore concluded that although crushing damage of concrete sleeper rail seats due to a single load application is not expected, crushing damage due to repeated load applications may be feasible in the presence of particle intrusion.

8. ACKNOWLEDGEMENTS

This research was primarily funded by Amsted RPS, who also supported the first two authors by a research grant. Additional support was provided by the National University Rail (NURail) Center, a US DOT-OST Tier 1 University Transportation Center. The published material in this report represents the position of the authors and not necessarily that of US DOT. Generous support and guidance has also been provided from the industry partners of this research: Union Pacific Railroad; BNSF Railway; National Railway Passenger Corporation (Amtrak); Amsted RPS / Amsted Rail, Inc.; GIC Ingeniería y Construcción; Hanson Professional Services, Inc.; and CXT Concrete Ties, Inc., and LB Foster Company. J. Riley Edwards has been supported in part by grants to the UIUC Rail Transportation and Engineering Center (RailTEC) from CN, CSX, Hanson Professional Services, and the George Krambles Transportation Scholarship Fund. For providing direction, advice, and resources, the authors would like to thank Christopher Rapp from Hanson Professional Services, Inc, Mauricio Gutierrez from GIC Ingeniería y Construcción, Professor Jerry Rose and Graduate Research Assistant Jason Stith from the University of Kentucky, and Vince Carrara from Tekscan®, Inc. The authors would also like to thank Tim Prunkard and the Civil and Environmental Engineering (CEE) Machine Shop from the University of Illinois at Urbana-Champaign for their assistance in laboratory experimentation, and undergraduate research assistant Zachary Jenkins for his assistance in analyzing the data presented in this paper.

REFERENCES

1. Zeman JC. Hydraulic mechanisms of concrete-tie rail seat deterioration. M.S. thesis. University of Illinois at Urbana-Champaign; 2010.
2. American Railway Engineering and Maintenance-of-Way Association. Manual for railway engineering. Lanham: AREMA; 2014.
3. Van Dyk BJ. Characterization of loading environment for shared-use railway superstructure in North America. M.S. thesis. University of Illinois at Urbana-Champaign; 2014.
4. Rapp CT, Dersch MS, Edwards JR, Barkan CPL, Wilson B, Mediavilla J. Measuring rail seat pressure distribution in concrete crossties: Experiments with matrix-based tactile surface sensors. Transportation Research Record: Journal of the Transportation Research Board, Transportation Research Board of the National Academies 2014; 2374: 190—200.
5. Greve MJ, Dersch MS, Edwards JR, Barkan CPL, Mediavilla J, Wilson B. Analysis of the relationship between rail seat load distribution and rail seat deterioration in concrete crossties. In: ASME. Joint Rail Conference, Colorado Springs, Colorado; 2014.
6. Greve MJ, Dersch MS, Edwards JR, Barkan CPL, Thompson HB, Sussman T, McHenry MT. Examination of the effect of concrete crosstie rail seat deterioration on rail seat load distribution. Accepted, Transportation Research Record: Journal of the Transportation Research Board, Transportation Research Board of the National Academies 2015.
7. Greve MJ, Dersch MS, Edwards JR, Barkan CPL. Evaluation of laboratory and field experimentation characterizing concrete crosstie rail seat load distributions. In: ASME. Joint Rail Conference, San Jose, California; 2015.
8. RailTEC. FRA improved concrete crossties and fastening systems for US high speed passenger rail and joint passenger/freight corridors. Railroad Transportation and Engineering Center (RailTEC), University of Illinois at Urbana-Champaign (UIUC). United States Department of Tranpsortation (USDOT) Federal Railroad Administration (FRA) Final Report, 2013.
9. Choros J, Coltman MN, Marquis B. Prevention of Derailments due to concrete tie rail seat deterioration. In: ASME. Joint Rail Conference & Internal Combustion Engine Spring Technical Conference, Pueblo, Colorado; 2007.
10. Rapp CR, Edwards JR, Dersch MS, Barkan CPL, Wilson B, Mediavilla J. Measuring concrete crosstie rail seat pressure distribution with matrix based tactile surface sensors. In: ASME. Joint Rail Conference, Philadelphia, PA; 2012.
11. Hay WW. Railroad engineering, second edition. New York: John Wiley & Sons, Inc.; 1982.
12. El Shahawi M, Batchelor BdV. Fatigue of partially prestressed concrete. Journal of Structural Engineering 1986; 112(3): 524—537.
13. ACI Committee 215. Considerations for design of concrete structures subjected to fatigue loading. Detriot (MI): American Concrete Institute; 1992 Nov.